Quantum formalism for electron capture from a solid surface by heavy projectiles making grazing collisions

J. E. Miraglia

Instituto de Astronomía y Física del Espacio, Consejo Nacional de Investigaciones Científicas y Técnicas, Casilla de Correo 67, Sucursal 28, 1428 Buenos Aires, Argentina

(Received 3 June 1993)

Electron capture from surfaces by grazing heavy projectiles is studied with a fully quantum treatment. The collision is considered in the high-energy regime where the projectile velocity is larger than the Fermi velocity of the free-electron gas of the solid. Some approximations commonly used in atomic collision theory, such as the first-order Born, the impulse, and the Vainstein-Presnyakov-Sovelman approximations, are adapted to the present geometry and interactions. The surface-electron and surface-projectile interactions are represented according to the jellium model and the Molière and Lindhard potentials. Detailed calculations are made for protons on an Al(111) surface and compared with recent experiments. No agreement is found; the theory largely underestimates the experiments at high energies. This disagreement shows that the high-energy-tail data cannot be explained as a capture process from the free-electron gas. Other neutralization mechanisms should take place to account for the experiments.

PACS number(s): 79.20.Rf

I. INTRODUCTION

During the past years there has been an increasing effort in the theoretical [1–4] and experimental [5, 6] fields of inelastic processes occurring with solid surfaces by impinging projectiles at grazing conditions. In the theoretical field, most of the investigators have tackled the problem with tools developed in their own fields, such as atomic collision theory. In the simplest and most ideal atomic collision, we generally deal with three particles: a projectile (P), an electron (e), and a target nucleus (T). Among the three collision velocity ranges, namely, low, intermediate, and high energies, the latter is the simplest to deal with. That is, the mechanisms involved are relatively simple and not numerous [7, 8]. Therefore, the understanding achieved in high-energy atomic collisions can be very useful in trying to understand inelastic grazing collisions at the simplest level.

If we translate an ideal atomic collision into an ion-surface process, we have again P and e, but instead of the point target T we now have the surface S. By S we mean not only the surface but also the whole solid (amorphous or crystalline) beneath the surface. Therefore, the simplest system is composed of two particles (P and e) and the solid structure (S). The neutralization can be read as follows: $P + (S^+ + e) \rightarrow (P + e) + S^+$. The job reduces to solving the problem under the new geometry and interactions.

In an interesting theoretical work, Thumm and Briggs (TB) [2] have presented an analysis of neutralization from a surface by grazing ion impact at high energies. The neutralization process has been envisaged as an electron capture process from the free-electron gas. Based on a classical description of the projectile and a quantum jellium model for the electron, these authors calculated the first and second perturbative orders to the probability. TB found that the second-order estimate is about two orders of magnitude greater than the first. The dominant mechanism was shown to be Thomas type [8] in which the electron first collides with the projectile and afterward, in a second step, it diffracts through the lattice atomic cores emerging from the surface with the same velocity as the projectile. This diffraction, found in the theory of TB, was related to the low-energy electron diffraction process (which resembles the Bragg law) producing steplike structures at the level of the total probability not found in the experiment [6].

In a recent article, Winter *et al.* [6] have measured the neutral fractions of protons scattered grazingly from an Al(111) surface carefully prepared. The impinging energies, ranging from 50 keV to 1.25 MeV, were typical of high energy; the incident angle was 3 mrad, i.e., as for grazing conditions. When compared with the theory of TB, no firm conclusion can be drawn since the data lie between the first and second perturbative orders. It is observed that the experiments do not show steplike structures as predicted by the Thomas-type process.

In this work, we study the capture process by heavy projectiles from crystal surfaces. Our formalism (developed in Sec. II) is fully quantum, not only for the electron, but also for the projectile. We would like to emphasize that a quantum picture is not very important to describe a heavy projectile as studied here, but a quantum treatment will certainly lead us to correct descriptions of all the momentum transfers involved. The crystal is considered as an ensemble of parallel planes. The S-e and S-P interactions are modeled in Sec. III after approximating the two-particle Molière and Lindhard potentials [9]; the jellium model is also studied. In Sec. IV, some approximations commonly used in atomic collision theory are applied (or adapted to the new geometry). These include the first-order Born approximation [12, 13] and a variation of this including the S-P interaction to all orders. Instead of the second-order Born ap-

proximation investigated by TB, we use two well-known theoretical methods used for three-particle atomic collisions, namely, the impulse [14, 15] and the Vainstein-Presnyakov-Sobelman [16] approximations. In Sec. V, we present the results, which are examined in Sec. V B after finding some closed forms to compare them with. Conclusions are presented in Sec. VI. We anticipate that none of the approximations developed here agrees with experiment [6]; capture from the free-electron gas is found to be very small. As explained in the following paper [17], the experiments can be explained as an electron capture process from *bound* electrons of atoms on the solid surface and not from the *free*-electron gas. The work is organized in such a way that the details of the calculations are presented in the Appendixes. Atomic units are used.

II. THE MODEL COLLISION

Let us consider a heavy projectile P of charge Z_P and mass M_P impinging on a solid crystal composed of an ensemble of horizontal parallel planes S and an electron e (by heavy projectile, we mean $M_P \geq M_0 = 1836$, with M_0 the proton mass). The projectile with initial momentum $\mathbf{K}_i$ captures an electron and the resulting atom emerges with final momentum $\mathbf{K}_f$ (see Fig. 1). The energy conservation reads

$$\frac{K_i^2}{2\nu_i} + \epsilon_i = \frac{K_f^2}{2\nu_f} + \epsilon_f, \tag{2.1}$$

where $\nu_i = M_P$, $\nu_f = M_P + 1$, and $\epsilon_{i,f}$ are the initial (bound to the solid) and final (bound to the projectile) electronic energies ($\epsilon_{i,f} < 0$). The mass of the surface is considered infinite; consequently the S-e and P-e reduced masses are $\mu_i = 1$ and $\mu_f = M_P/(M_P + 1)$. The initial and final momenta are

$$\begin{aligned} \mathbf{K}_i &= (K_{ix},\ K_{iy},\ K_{iz}) = K_i\ (\sin\theta_i,\ 0, -\cos\theta_i), \\ \mathbf{K}_f &= (K_{fx},\ K_{fy},\ K_{fz}) \\ &= K_f\ (\sin\theta_f \cos\varphi_f, \sin\theta_f \sin\varphi_f, \cos\theta_f). \end{aligned} \tag{2.2}$$

The coordinate systems are chosen in the usual way of atomic collision theory (see Fig. 2): $(\mathbf{R}_i, \mathbf{r}_i)$ and $(\mathbf{R}_f, \mathbf{r}_f)$, and the corresponding reduced masses are (ν_i, μ_i) and (ν_f, μ_f), respectively. Due to the geometry of our problem, it is convenient to separate all the coordinates into components parallel and perpendicular to the surface (see Fig. 2); in this way we have $\mathbf{R}_i = (\mathbf{R}_{is},\ Z_i)$, $\mathbf{R}_f = (\mathbf{R}_{fs},\ Z_f)$, $\mathbf{r}_i = (\mathbf{r}_{is},\ z_i)$, and $\mathbf{r}_f = (\mathbf{r}_{fs},\ z_f)$. The components $\mathbf{R}_{(i,f)s}$ and $\mathbf{r}_{(i,f)s}$ are parallel to the surface and $Z_{i,f}$ and $z_{i,f}$ are perpendicular to the surface.

We write the Hamiltonian of P, S, and e as

$$\begin{aligned} H &= -\frac{1}{2\nu_i}\nabla^2_{\mathbf{R}_i} - \frac{1}{2\mu_i}\nabla^2_{\mathbf{r}_i} + V_{Se}(\mathbf{r}_i) + V_{SP}(\mathbf{R}_i) + V_{Pe}(\mathbf{r}_f) \\ &= -\frac{1}{2\nu_f}\nabla^2_{\mathbf{R}_f} - \frac{1}{2\mu_f}\nabla^2_{\mathbf{r}_f} + V_{Se}(\mathbf{r}_i) + V_{SP}(\mathbf{R}_i) + V_{Pe}(\mathbf{r}_f) = H_i + V_i = H_f + V_f\ , \end{aligned} \tag{2.3}$$

with $V_i = V_{Pe} + V_{SP}$ and $V_f = V_{Se} + V_{SP}$. According to the symmetry chosen we have the S-P interaction $V_{SP}(\mathbf{R}_i) = V_{SP}(Z_i)$, the S-e interaction $V_{Se}(\mathbf{r}_i) = V_{SP}(z_i)$, and the P-e Coulomb potential $V_{Pe}(\mathbf{r}_f) = -Z_P/r_f$.

The transition-matrix element reads

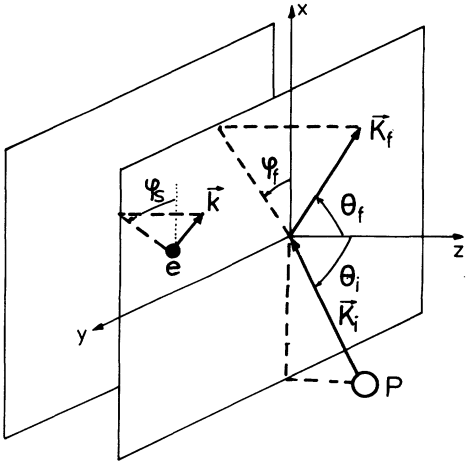

FIG. 1. Schematic diagram of the momenta involved.

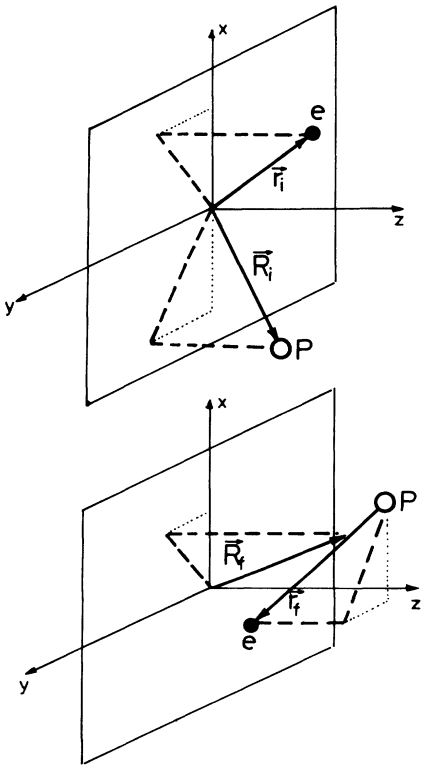

FIG. 2. Schematic diagram of the coordinate systems.

$$T = \langle \psi_f | V_f | \Psi_i^+ \rangle = \langle \Psi_f^- | V_i | \psi_i \rangle \ , \tag{2.4}$$

where the unperturbed (Born) wave functions are given in the usual form:

$$\psi_i = \frac{\exp(i\mathbf{K}_i \cdot \mathbf{R}_i)}{(2\pi)^{3/2}} \ \phi_i(\mathbf{r}_i), \ \ \psi_f = \frac{\exp(i\mathbf{K}_f \cdot \mathbf{R}_f)}{(2\pi)^{3/2}} \ \phi_f(\mathbf{r}_f) \ , \tag{2.5}$$

and $\Psi_{i,f}^{\pm}$ are the (generally unknown) exact wave functions. Following TB [2], the electron-gas wave function $\phi_i(\mathbf{r}_i)$ characterized with the initial momentum $\mathbf{k}$ can be separated into two components, namely, a transverse (in terms of $\mathbf{r}_{is}$) and a longitudinal (in terms of z_i) function:

$$\phi_i(\mathbf{r}_i) = \frac{\exp(i\mathbf{k}_s \cdot \mathbf{r}_{is})}{(2\pi)} \ \phi_{k_z}^+(z_i) \ , \tag{2.6}$$

where we decompose $\mathbf{k} = (\mathbf{k}_s, k_z) = (k_s \cos\varphi_s, k_s \sin\varphi_s, k_z)$, and $\mathbf{k}_s$ and k_z are the components of the electron momentum $\mathbf{k}$, respectively, parallel and perpendicular to the surface. Due to this separation of coordinates, we can always write

$$T = \delta(\mathbf{W}_{is} - \mathbf{k}_s) \ \tau, \tag{2.7}$$

where τ is now a one-dimensional transition-matrix element in the $\{z, Z\}$ space given by

$$\tau = \langle \psi_{fL} | V_f | \Psi_{iL}^+ \rangle = \langle \Psi_{fL}^- | V_i | \psi_{iL} \rangle \ . \tag{2.8}$$

The suffix L in the subscript indicates the corresponding one-dimensional wave functions. In Sec. IV, we will present these linear functions depending on the particular approximation used. The momentum transfer vectors $\mathbf{W}_{i,f}$ are defined in the usual way of atomic collision theory: $\mathbf{W}_i = \mathbf{K}_f - \mathbf{K}_i$, $\mathbf{W}_f = \mathbf{K}_i - \mu_f \mathbf{K}_f$, satisfying

$$\mathbf{W}_i + \mathbf{W}_f = \frac{\mathbf{K}_f}{\nu_f} = \mathbf{v}_f, \quad \mathbf{W}_f + \mu_f \mathbf{W}_i = \frac{\mu_f \mathbf{K}_i}{\nu_i} = \mu_f \mathbf{v}_i, \tag{2.9}$$

$$\frac{W_i^2}{2} - \epsilon_i = \frac{W_f^2}{2\mu_f} - \epsilon_f. \tag{2.10}$$

ϵ_i is given by $\epsilon_i = -V_{Ce} + k^2/2$, $V_{Ce} = E_F + E_W$ is the confinement energy, E_F is the Fermi energy, and E_W is the work function. We separate $\mathbf{W}_i = (\mathbf{W}_{is}, W_{iz})$, $\mathbf{W}_f = (\mathbf{W}_{fs}, W_{fz})$, $\mathbf{v}_i = (\mathbf{v}_{is}, v_{iz})$, and $\mathbf{v}_f = (\mathbf{v}_{fs}, v_{fz})$, where the subscripts ending with s and z represent, respectively, the parallel and perpendicular components to the surface. Due to the momentum conservation in the surface direction [Eq. (2.7)] we have $\mathbf{W}_{is} = \mathbf{k}_s$ and $\mathbf{W}_{fs} = \mathbf{v}_f - \mathbf{k}_s$.

A. The probability of transition

The total probability of electron capture is defined as the probability per unit time integrated over the density of final states $d\mathbf{K}'_f = K'^2_f \sin\theta'_f \, dK'_f \, d\theta'_f \, d\varphi'_f$ divided by the density flux J_i perpendicular to the surface, i.e.,

$$P(\mathbf{k}) = \frac{1}{J_i} \int d\mathbf{K}'_f \ 2\pi \ \delta\left(\frac{K'^2_f}{2\nu_f} - \frac{K_i^2}{2\nu_i} - \epsilon_i + \epsilon_f\right) \times \delta^2(\mathbf{W}_{is} - \mathbf{k}_s) \ |\tau|^2 \ . \tag{2.11}$$

The first δ function gives the energy conservation fixing the value of $|\mathbf{K}_f|$ in accordance with Eq. (2.1).

The object δ^2 is very common in the formal theory of scattering [18] where it takes into account the conservation of linear momentum [19]. The manipulation of the distribution δ^2 requires some explanation, as indicated next. Following the formal theory of scattering, we should prepare the incident incoming particle and the electron wave function $\phi_i(\mathbf{r}_i)$ [Eq. (2.5)] with wave packets. After the collision, we should integrate on the corresponding distributions and, in this way, one finds that $\delta^2(\mathbf{W}_{is} - \mathbf{k}_s)$ reduces to $\delta(\mathbf{W}_{is} - \mathbf{k}_s)$. An equivalent and simple way of dealing with the distribution δ^2 is the prescription of Joachain [19] to deal with the on-the-momentum-shell transition matrix, as summarized next. By using wave packets, we find $\delta(\mathbf{W}_{is} - \mathbf{k}_s)\delta(\mathbf{W}_{is} - \mathbf{k}'_s)$ instead of $\delta^2(\mathbf{W}_{is} - \mathbf{k}_s)$, where $\mathbf{k}'_s$ is the variable introduced by the wave packet. Using the identity $\delta(\mathbf{W}_{is} - \mathbf{k}_s)\delta(\mathbf{W}_{is} - \mathbf{k}'_s) = \delta(\mathbf{W}_{is} - \mathbf{k}_s)\delta(\mathbf{k}_s - \mathbf{k}'_s)$ and integrating with respect to $\mathbf{k}'_s$, the distribution $\delta(\mathbf{k}_s - \mathbf{k}'_s)$ is finally removed. We can then write

$$P(\mathbf{k}) = (2\pi) \ \frac{\nu_i \nu_f \ K_f}{J_i} \int d\varphi'_f \ d\theta'_f \sin\theta'_f \ \delta(\mathbf{W}_{is} - \mathbf{k}_s) \ |\tau|^2. \tag{2.12}$$

The δ function fixes φ'_f and θ'_f to give two possibilities for a given value of $\mathbf{k}_s$. In other words, the angular distribution (differential probability) is composed of two δ functions producing

$$P(\mathbf{k}) = P^-(\mathbf{k}) + P^+(\mathbf{k}) \tag{2.13}$$

at the angles

$$\cos\theta_f^{\pm} = \pm \left[1 - \frac{(K_i \sin\theta_i + k_s \cos\varphi_s)^2 + (k_s \sin\varphi_s)^2}{K_f^2}\right]^{1/2},$$

$$\tan\varphi_f = \frac{k_s \sin\varphi_s}{K_i \sin\theta_i + k_s \cos\varphi_s} \ . \tag{2.14}$$

The first term $P^-(\mathbf{k})$ is the *transmitted* probability where the projectile is scattered at $\{\varphi_f, \ \theta_f^-\}$, i.e., it penetrates the surfaces under consideration. The probability $P^-(\mathbf{k})$ is relevant where the component of the energy along the z axis is *larger* than the repulsion barrier. Here we have

$$W_{iz}^- = K_f \cos\theta_f^- + K_i \cos\theta_i,$$
$$W_{fz}^- = -K_i \cos\theta_i - \mu_f K_f \cos\theta_f^- . \tag{2.15}$$

The second term in Eq. (2.13) $P^+(\mathbf{k})$ is the *grazing* collision, where the projectile is scattered at $\{\varphi_f, \ \theta_f^+\}$, i.e., it

returns without penetrating the solid (see Fig. 1). $P^+(\mathbf{k})$ is simply the integration of the δ function at φ_f and θ_f^+, and it is the one we are interested in. The probability $P^+(\mathbf{k})$ is relevant where the component of the energy along the z axis is *smaller* than the repulsion barrier. The z coordinates of the momentum transfer vectors are, in this case,

$$W_{iz}^+ = K_f \cos\theta_f^+ + K_i \cos\theta_i = (M_P + 1)v_{fz} + M_P|v_{iz}|, \tag{2.16}$$

$$W_{fz}^+ = -K_i \cos\theta_i - \mu_f K_f \cos\theta_f^+ = -M_P(v_{fz} + |v_{iz}|).$$

For grazing collision, we have $v_{iz} < 0$, $v_{fz} > 0$, and

$$v_{fz}^2 = \mu_f v_{iz}^2 + \frac{2}{M_P + 1}\left[\epsilon_{iz} - \epsilon_f + \tfrac{1}{2}(\mathbf{v}_{fs} - \mathbf{k}_s)^2\right], \tag{2.17}$$

with $\epsilon_{iz} = -V_{Ce} + k_z^2/2$. A very important point that should be noted from Eq. (2.17) is the inequality $v_{fz} > |v_{iz}|$, which makes the reflection angle with respect to the surface larger than the incident angle. For instance, for the case observed by Winter *et al.* (Ref. [6], Fig. 1), corresponding to 525 keV protons impinging at 3 mrad with respect to the Al surface ($v_{iz} = -0.0137$), Eq. (2.17) gives $v_{fz} \approx 8|v_{iz}|$. This is a very important difference in relation to the semiclassical specular description where $v_{fz} = -v_{iz}$ is assumed.

After some algebra with δ functions, we find from Eq. (2.12)

$$P^{\pm}(\mathbf{k}) = \frac{(2\pi)\nu_i\nu_f}{J_i\ K_f|\cos\theta_f|}|\tau^{\pm}|^2 = \frac{(2\pi)^2}{|v_{iz}v_{fz}|}\ |\tau^{\pm}|^2\ , \tag{2.18}$$

where $\tau^{\pm}$ is the one-dimensional transition matrix calculated with $W_{(i,f)z}^{\pm}$. Equation (2.18) has a similar form to that of the one-dimensional capture process studied by Dettmann and Leibfried [Ref. [20], Eq. (9a)]. Equation (2.18) holds if θ_f is real; otherwise $P^{\pm}(\mathbf{k}) = 0$. Imaginary θ_f implies that energy and momentum are not conserved. It is interesting to note that when $\cos\theta_f = 0$, $P^{\pm}$ presents a singularity, and this is because the final atom finishes *trapped* on the surface. This situation is in between transmission and grazing collisions.

Finally, the total probability, integrated over the whole electron gas momentum distribution, is given by

$$P^{\pm} = 2\int_0^{2\pi} d\varphi_s \int_{-k_F}^{+k_F} d\ k_z \int_0^{(k_F^2 - k_z^2)^{1/2}} dk_s\ k_s P^{\pm}(\mathbf{k})\ , \tag{2.19}$$

where $k_F = (2\ E_F)^{1/2}$. The factor 2 in front of the integral accounts for the two states of the spins.

It should be noted that if the final velocity parallel to the surface is much larger than the Fermi velocity, i.e., $v_{fs} \gg k_s$, then τ becomes independent of φ_s and the integral on the azimuth can be performed to give a closed form in terms of the complete elliptic integral **K**.

From now on, we shall concentrate on grazing collisions and the superscript + will be omitted.

III. THE MODEL POTENTIALS

In this section, we proceed to model the *S-e* and *S-P* potentials. In Appendix A, we study two simple solutions of the Thomas-Fermi potential of a Coulomb charge interacting with an atom, namely, the Molière and Lindhard closed-form potentials [9]. Also the Hartree-Fock static potential was calculated. After integrating the effect of the whole surface, we fitted them with exponential and Coulomb-type one-dimensional potentials valid at short and medium (but not very large) distances (Fig. 3). In a more general and accurate case, we can use a more sophisticated interatomic potential, make the surface integration [Eq. (A1)], and then fit it with a potential, preferably having a known solution of the corresponding Schrödinger equation.

A. Surface-electron potential

The most elemental interaction has been proposed by TB [2]:

$$V_{Se}^J(z) = \begin{cases} -V_{Ce}, & z < 0 \\ 0, & z > 0\ . \end{cases} \tag{3.1}$$

This is called the jellium model and it has the great advantage of having closed forms, not only for the wave function but also for the first-order T-matrix element. This model will serve us as a useful reference.

For the short range Molière II potential (see Appendix A for details), we propose

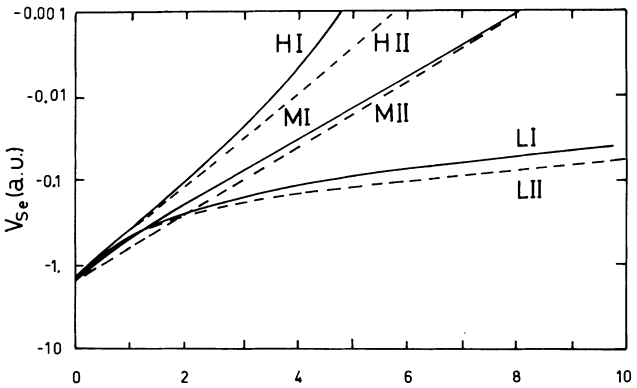

FIG. 3. Surface-electron interaction as a function of the distance. The surface considered corresponds to an Al crystal. Solid lines correspond to the Molière I (MI) and Lindhard I (LI) expressions [Eq. (A3)] and the Hartree-Fock static potential (HI). Dashed lines correspond to the Molière II and Lindhard II approximate expressions [Eq. (A4)] with $\kappa_m = 0.917$ and $\kappa_l = 2.14$, respectively. Also the surface-electron Hartree-Fock static potential is shown by a solid line (HI) and the approximated formula $1.4\exp(-1.3\ Z)$ is shown by a dashed line (HII).

$$V_{Se}^{M}(z) = -V_{Se0} \sum_{j=0}^{\infty} \exp\left[-\kappa_m |z + jd|\right], \tag{3.2}$$

where V_{Se0} and κ_m are defined in Appendix A [10].

For a long range potential, such as the Lindhard II (see Appendix A), we propose

$$V_{Se}^{L}(z) = \begin{cases} -V_{Se0}\left[1 + \kappa_l z\right]^{-1}, & z > 0, \\ -V_{Se0} \sum_{j=0}^{\infty} \left[1 + \kappa_l |z + jd|\right]^{-1} \Theta_d(z + jd), & \end{cases}$$

$$z < 0, \tag{3.3}$$

where the cutoff function $\Theta_d(z) = 1$ if $|z| < d$ and zero otherwise. In Fig. 4, we plot the model potentials.

B. Surface-projectile potential

To start, we can describe the broken line trajectory posed by TB [2] by considering an unpenetrable barrier at Z_0, Z_0 being the distance of closest approach,

$$V_{SP}^{J}(Z) = \begin{cases} \infty, & Z < Z_0 \\ 0, & Z > Z_0 \end{cases}. \tag{3.4}$$

For Molière II and Lindhard II potentials, to be consistent with the preceding subsection, we use the same expressions as Eqs. (3.2) and (3.3) with V_{SP0}, κ_M, and κ_L instead of V_{Se0}, κ_m, and κ_l. We consider $V_{SP0} = -Z_P V_{Se0}$, $\kappa_M = \kappa_m$, and $\kappa_L = \kappa_l$. However, other values of V_{SP0}, κ_M, and κ_L can be used instead if there are solid physical arguments to support them.

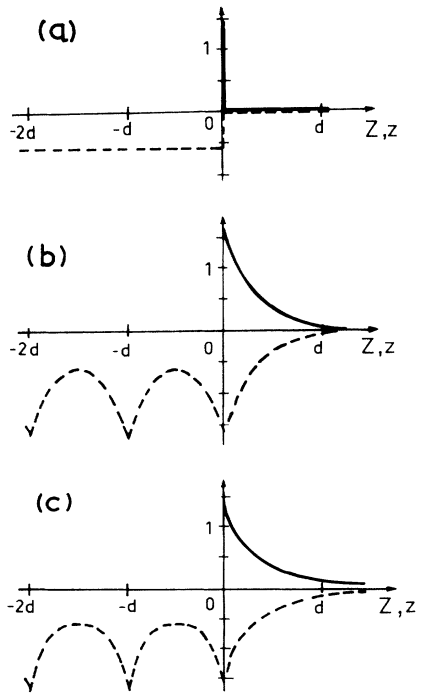

FIG. 4. Electron-surface (dashed lines) and proton-surface (solid lines) potentials as a function of the distances z and Z, respectively, for (a) jellium, (b) the Molière model, and (c) the Lindhard model.

The quantum treatment of the projectile also takes into account tunnel penetration, which is neglected in a classical description, including intermediate planar channeling. Anyway, for grazing incidence the description of the S-P interaction well within the solid should not be very important, even less if the projectiles are heavy ions as in our case. Therefore, to simplify our calculation, we have considered only the outside part of the potential ($Z > 0$) and let it be zero otherwise, as shown in Fig. 4 [see also Eq. (C2) and discussions below].

In summary, besides the well-known jellium model, we have introduced in this section two other models based on the simple-form Molière II and Lindhard II potentials. Accordingly, we will designate as Molière and Lindhard models the ones describing the S-e attractive interactions by Eqs. (3.2) and (3.3), respectively, and the equivalent expressions to describe the S-P repulsive interactions. In Fig. 4, we show a schematic picture of the potentials involved in each model.

IV. APPROXIMATIONS

In this section, we proceed to use the time-independent distorted wave formalism to solve the Schrödinger equation. For simplicity, we consider heavy projectiles. We shall investigate several theoretical methods: the first-order Born approximation to start with and two distorted wave methods based on the impulse approximation to take into account higher perturbative orders.

A. First-order Born approximation

By first-order Born approximation, we mean the first perturbative order to the T matrix in the residual potentials, either V_i or V_f.

1. *Brinkman-Kramers approximation*

The most elemental approximation in an electron capture process is the neglect of the internuclear interaction, V_{SP} in our case (i.e., $V_f \approx V_{Se}$), to give $T_{BK} = \langle \psi_f | V_{Se} | \psi_i \rangle$ or $\tau_{BK} = \langle \psi_{fL} | V_{Se} | \psi_{iL} \rangle$. This is called the Brinkman-Kramers (BK) approximation [12]. Although, as we shall see, its contribution is irrelevant for grazing collisions involving heavy projectiles, it provides very useful insight of the profiles and basic parameters involved in the collision. After simple algebra, we find the following one-dimensional wave functions:

$$\psi_{iL} = \frac{\exp\left(iK_{iz}Z_i\right)}{(2\pi)^{1/2}} \phi_{k_z}^{+}(z_s), \tag{4.1}$$

$$\psi_{fL} = \frac{\exp\left(iK_{fz}Z_f\right)}{(2\pi)^{1/2}} \phi_f(\mathbf{v}_{fs} - \mathbf{k}_s | z_f),$$

where $\phi_f(\mathbf{v}_{fs} - \mathbf{k}_s | z_f)$ is a one-dimensional profile of the final wave function $\phi_f(\mathbf{r}_f)$ expressed in terms of a two-dimensional Fourier transform. In Eq. (4.1), $Z_{i,f}$ is the

component of $\mathbf{R}_{(i,f)}$ perpendicular to the surface. In general, for a given function in the coordinate space $\mathbf{r}$ $\mathcal{F}(\mathbf{r})$ and its three-dimensional Fourier transform $\tilde{\mathcal{F}}(\mathbf{K})$ in the momentum space $\mathbf{K}$, we denote the partial or one-dimensional Fourier transform as

$$\mathcal{F}(\mathbf{K}_s|z) = \int \frac{d\mathbf{r}_s}{2\pi} \exp(-i\mathbf{K}_s.\mathbf{r}_s)\mathcal{F}(\mathbf{r}) = \int_{-\infty}^{+\infty} \frac{dK_z}{(2\pi)^{1/2}} \exp(iK_z z)\tilde{\mathcal{F}}(\mathbf{K}_s, K_z), \tag{4.2}$$

where $\mathbf{r} = (\mathbf{r}_s,\ z)$, $\mathbf{K} = (\mathbf{K}_s, K_z)$, etc. Conversely,

$$\tilde{\mathcal{F}}(\mathbf{K}) = \int \frac{d\mathbf{r}}{(2\pi)^{3/2}} \exp(-i\mathbf{K}\cdot\mathbf{r})\mathcal{F}(\mathbf{r}) = \int_{-\infty}^{+\infty} \frac{dz}{(2\pi)^{3/2}} \exp(-iK_z z)\mathcal{F}(\mathbf{k}_s|z). \tag{4.3}$$

For a pure Coulomb potential, and for the ground state, the profile or one-dimensional wave function is given by

$$\phi_{1s}(\mathbf{K}|z) = \frac{Z_P^{5/2}\ \exp\left(-z(Z_P^2+K^2)^{1/2}\right)}{\pi^{1/2}\ (Z_P^2+K^2)} \times \left[z + \frac{1}{(Z_P^2+K^2)^{1/2}}\right], \tag{4.4}$$

satisfying a one-dimensional Schrödinger equation with a linear pseudopotential

$$-\frac{Z_P^2+K^2}{1+z\ (Z_P^2+K^2)^{1/2}}\ . \tag{4.5}$$

Note that this linear potential is Coulombic at large but finite distances as $z \to 0$.

After using the Schrödinger equation in momentum space,

$$\tilde{I}_k(W) = \int_{-\infty}^{+\infty} \frac{du}{(2\pi)^{1/2}} \tilde{\phi}_k^+(u)\ \tilde{V}_{Se}(W-u) = \left(\epsilon_{iz} - W^2/2\right)\tilde{\phi}_k^+(W) \tag{4.6}$$

$$= \int_{-\infty}^{+\infty} \frac{dz}{(2\pi)^{1/2}} \exp(-iWz)\ \phi_k^+(z)\ V_{Se}(z), \tag{4.7}$$

we can write the first-order BK in closed form:

$$\tau_{BK} = \tilde{\phi}_f^*(\mathbf{W}_f)\tilde{I}_{k_z}(W_{iz}) = \tilde{\phi}_f^*(\mathbf{W}_f)\left[\epsilon_{iz} - W_{iz}^2/2\right]\tilde{\phi}_{k_z}^+(W_{iz}), \tag{4.8}$$

where $\mathbf{W}_f = (\mathbf{W}_{fs}, W_{fz}) = (\mathbf{v}_{fs} - \mathbf{k}_s, W_{fz})$, W_{iz} and W_{fz} are given in Eq. (2.16), and the asterisk denotes the conjugation operation. Equation (4.8) has the same structure as the atomic collision counterpart [20]. In Appendix B, we evaluate the magnitude $\tilde{I}_{k_z}$.

Our experience in atomic collisions teaches us that at backward angles the first-order BK is negligible. The dominant interaction is the internuclear interactions, translated here as V_{SP}, not considered in the BK approximation. Mathematically, it can be seen that for a $1s$ final state $\tau_{BK} \propto \tilde{\phi}_f^*(\mathbf{W}_f) \propto W_{fz}^{-2} \propto M_P^{-2}$. As we shall see in Sec. V, the matrix element including V_{SP} produces a dependence M_P^{-1}. Therefore we expect the BK to be important for the transmitted or forward capture but irrelevant for grazing collisions or backward capture.

2. *Jackson-Schiff or first-order Born approximation*

Certainly, the first order includes the S-P term $\langle\psi_{fL}|V_{SP}|\psi_{iL}\rangle$, which cannot be neglected for grazing collisions. The full first order is then

$$\tau_{B1} = \langle\psi_{fL}|V_{Se} + V_{SP}|\psi_{iL}\rangle \tag{4.9}$$

$$= \tau_{BK} + \int \frac{du}{(2\pi)^{1/2}} \tilde{V}_{SP}(u)\ \tilde{\phi}_f^*(\mathbf{v}_{fs} - \mathbf{k}_s|W_{fz}+u) \times \tilde{\phi}_{k_z}^+(W_{iz}-u)\ . \tag{4.10}$$

and τ_{BK} is negligible, as mentioned before. The integral over u is a variant of the Feynman integral and it represents the Jackson-Schiff approximation [13] in the traditional capture formalism. Note that it is fully equivalent to the one-dimensional integral obtained by Dettmann and Leibfried in their one-dimensional model [Ref. [20] Eq. (16)]. For numerical reasons that will become evident later, we re-write the preceding equation as

$$\tau_{B1} = \int \frac{du}{(2\pi)^{1/2}} \tilde{D}_{B1}(u)\ \tilde{\phi}_f^*(\mathbf{v}_{fs} - \mathbf{k}_s|W_{fz}+u) \times \tilde{I}_{k_z}(W_{iz}-u)\ , \tag{4.11}$$

where we have used Eq. (4.6) and

$$\tilde{D}_{B1}(u) = \tilde{V}_{SP}(u)\frac{-2}{(W_{iz}-u)^2 - 2\epsilon_{iz}}. \tag{4.12}$$

The Fourier transforms of the potentials are displayed in Appendix C.

B. Surface Born approximation

It is obvious that the S-P interaction is essential to describe the projectile reflection and in this way the capture process. The S-P interaction should then be treated to all orders by building up this interaction in the corresponding wave functions. Atomic collision approximations related to this method are, for example, the Coulomb Born approximation in the electron-atom excitation [21] and the Coulomb Brinkman-Kramers approximation [22] for capture. In a similar fashion to these approximations, we distort the projectile plane wave in Eq. (4.1) by the full S-P continuum, namely,

$$\Phi_{K_{iz}}^+(V_{SP0}, Z_i) = \frac{\exp(iK_{iz}Z_i)}{(2\pi)^{1/2}}\ D_{SP}^+(V_{SP0}, K_{iz};\ Z_i)\ , \tag{4.13}$$

$$\Phi_{K_{fz}}^-(V_{SP0}, Z_f) = \frac{\exp(iK_{fz}Z_f)}{(2\pi)^{1/2}}\ D_{SP}^-(V_{SP0}, K_{fz};\ Z_f)\ .$$

The distorting factors $D^{\pm}_{SP}$ are evaluated in Appendix C. The corresponding T matrix, which we will call surface first-order Born (SB1), is then

$$\tau_{\rm SB1} = \langle \psi_{fL} D^{-}_{SP}(V_{SP0}) | V_{Se} | \psi_{iL} D^{+}_{SP}(V_{SP0}) \rangle$$

$$= \langle \Phi^{-}_{K_{fz}}(V_{SP0}) \phi_f(\mathbf{v}_{fs} - \mathbf{k}_s) | V_{Se} | \Phi^{+}_{K_{iz}}(V_{SP0}) \phi^{+}_{k_z} \rangle$$

$$= \int \frac{du}{(2\pi)^{1/2}} \tilde{D}_{\rm SB1}(u) \tilde{\phi}^{*}_f(\mathbf{v}_{fs} - \mathbf{k}_s | W_{fz} + u) \times \tilde{I}_{k_z}(W_{iz} - u), \tag{4.14}$$

where $\tilde{D}_{\rm SB1}(u)$ is the Fourier transform of the function

$$D_{\rm SB1}(Z_i) = D^{+}_{\rm SP}(V_{\rm SP0}, K_{iz};\ Z_i)\ D^{-*}_{SP}(V_{SP0}, K_{fz};\ Z_f) \tag{4.15}$$

and where we have assumed $Z_f \approx Z_i$ since we will be dealing with heavy projectiles. In Appendix C, we present details of the calculation of $D_{\rm SB1}(Z_i)$. Note that if the S-P interaction is dropped, then we obtain $D_{\rm SB1}(Z_i) = 1$ and $\tilde{D}_{\rm SB1}(u) = (2\pi)^{1/2}\delta(u)$, recovering the first-order BK approximation, as expected.

The function $D_{\rm SB1}(Z)$ has an equivalent counterpart in three-particle atomic collision theory representing the internuclear distortion, namely, the well-known factor $\exp[(2iZ_TZ_P/v)\ln\rho]$, where ρ is the impact parameter [see, for example, the striking similarity to Eq. (C10)]. Mathematically, the oscillatory behavior as $\rho \to 0$ cancels the contribution at close distances; physically, it can be ascribed to the internuclear repulsion. A similar interpretation applies for $D_{\rm SB1}(Z)$. In Fig. 5, we plot real (Re) and imaginary (Im) parts of $D_{\rm SB1}(Z)$ as a function of Z [see Eq. (C6)] for protons colliding with on an Al crystal at 525 keV (corresponding to Fig. 1 of Ref. [6]) considering the Molière model. The oscillations as $Z \to 0$ cancel the exchange contributions at P-S distances shorter than the turning point Z_0. This effect is well known in planar channeling where a classical cut-off function is generally used to neglect P-S distances shorter than Z_0, which is unity for $Z > Z_0$ and zero for $Z < Z_0$ [23]. This crude approximation is essentially the "unpenetrable wall model," which we study in Appendix C. This simple model should be equivalent to the broken classical trajectory used by TB [2].

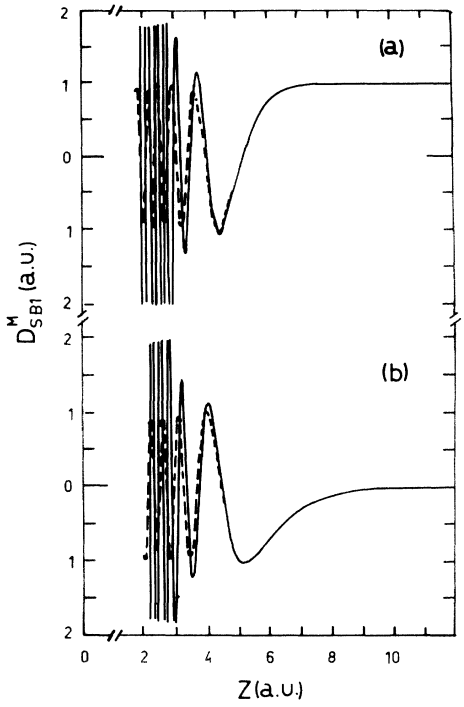

FIG. 5. Plot of (a) real and (b) imaginary parts of $D_{\rm SB1}$ as a function of Z for 525 keV protons colliding with an Al crystal at 3 mrad (corresponding to Fig. 1 of Ref. [6]) within the Molière model. Solid lines, expression Eq. (C5); dashed lines, the eikonal approximation Eq. (C6). The parameters are $V_{SP0} = 1.66$, $\kappa_m = 0.917$, $k = 0$, and the distance of closest approach or turning point is 2.46 a.u.

C. Surface impulse approximation

In the three-particle atomic collision theory, the impulse approximation considers the distortion of the electron cloud by the projectile, neglecting the forces due to the target nucleus. The simplest application to our case consists of distorting the initial wave function ψ_i by

$$\psi^{\rm SI}_i = \psi_i\ D^{+}_{SP}(V_{SP0}, K_{iz};\ Z_i)\ D^{+}_{Pe}(Z_P, \mathbf{v}_r;\ \mathbf{r}_P)\ , \tag{4.16}$$

where $\mathbf{v}_r$ is the relative velocity of the electron with respect to the projectile, $\mathbf{v}_r = \mu_f(\mathbf{k} - \mathbf{v}_i) = (\mathbf{v}_{rs}, v_{rz}) = \mu_f(\mathbf{k}_s - \mathbf{v}_{is},\ k_z - v_{iz})$, and $D^{+}_{\rm Pe}$ is the well-known Coulomb distortion factor given by

$$D^{+}_{Pe}(Z_p, \mathbf{v}_r;\ \mathbf{r}) = \exp(\pi a_P/2)\ \Gamma(1 - ia_P)\,{}_1F_1(+ia_P,\ 1;\ iv_r r - i\mathbf{v}_r \cdot \mathbf{r})\ , \tag{4.17}$$

with $a_P = Z_P/v_r$.

In fact, this approximation is not the *exact* impulse approximation but a *peaking* version. Its validity in the present case should be very high because the impact velocity considered here is much larger than the Fermi velocity of the electrons in the solid. We construct the surface impulse (SI) approximation as

$$\tau_{\rm SI} = \langle \Phi^{-}_{K_{fz}}(V_{SP0}) F_f(\mathbf{v}_{fs} - \mathbf{k}_s) | V_{Se} | \Phi^{+}_{K_{iz}}(V_{SP0}) \phi^{+}_{k_z} \rangle$$

$$= \int \frac{du}{(2\pi)^{1/2}} \tilde{D}_{\rm SI}(u)\ \tilde{F}^{*}_f(\mathbf{v}_{fs} - \mathbf{k}_s | W_{fz} + u)\ \tilde{I}_{k_z}(W_{iz} - u), \tag{4.18}$$

$$F_f(\mathbf{r}_f) = \phi_f(\mathbf{r}_f)\ D_P^{+\,*}(Z_P, \mathbf{v}_r;\ \mathbf{r}_P) = \phi_f(\mathbf{r}_f)\ D_{Pe}^{-}(Z_P, -\mathbf{v}_r;\ \mathbf{r}_P), \tag{4.19}$$

and $\tilde{D}_{\rm SI} = \tilde{D}_{\rm SB1}$. Here the function $F_f(\mathbf{v}_{fs}-\mathbf{k}_s|z_f)$ plays the role of a one-dimensional final state just as $\phi_f(\mathbf{v}_{fs}-\mathbf{k}_s|z_f)$ does in the SB1 approximation in Eq. (4.14). For a $1s$ final state we can write

$$\tilde{F}_{1s}^{*}(\mathbf{v}_{fs}-\mathbf{k}_s|W_{fz}+u)\ = \tilde{\phi}_{1s}^{*}(\mathbf{v}_{fs}-\mathbf{k}_s|W_{fz}+u)\ M_{1s}(u)\ , \tag{4.20}$$

with the modulating function

$$M_{1s}(u)\ = \exp(\pi a_P/2)\ \Gamma(1-ia_P)\ A_P^{-ia_P}\left[(1-ia_P)+\frac{1+ia_P}{A_P}\right], \tag{4.21}$$

$$A_P = \frac{(\mathbf{v}_{fs}-\mu_f\mathbf{v}_{is}-(M_P+1)^{-1}\mathbf{k}_s)^2\ +\ (\mu_f(k_z-W_{iz})+u)^2-(v_r+iZ_P)^2}{(\mathbf{v}_{fs}-\mathbf{k}_s)^2+(W_{fz}+u)^2+Z_P^2}. \tag{4.22}$$

Note that the presence of $M_{1s}(u)$ is the only difference with respect to the SB1 calculation.

D. Surface Vainstein-Presnyakov-Sobelman approximation

In relation to the SI approximation, it may be argued that for proton impact the S-P interaction cancels the S-e interacting at large distances in the final channel. So to satisfy the asymptotic conditions, for proton impact, for example, one should better use simply the unperturbed (Born) wave function. We are here revisiting a situation very well-known in three-particle atomic collision theory, where one has to deal with a large range potential. In this respect, we should recall some boundary-corrected perturbative approximations such as the true [24] and boundary [25] first-order Born approximations. In our case, however, we are correcting short range potentials and so we do not expect large corrections to the SI approximation. The theory that we propose here is termed the surface Vainstein-Presnyakov-Sobelman (SVPS), originally developed in the context of electron-atom collisions 30 years ago [16].

The initial wave function used in this model is again $\psi_i^{\rm SI}$, as in Eq. (4.16), and the final is

$$\psi_f^{\rm SVPS} = \psi_f D_{SP}^{-}(V'_{SP0}, K_{fz};\ Z_f), \tag{4.23}$$

with $V'_{SP0} = (Z_P-1)V_{SP0}/Z_P$. The remaining perturbation is therefore $V_{Se}+V_{SP}/Z_P$ and after some algebra we find

$$\begin{aligned}\tau_{\rm SVPS} &= \langle \Phi_{K_{fz}}^{-}(V'_{SP0})F(\mathbf{v}_{fs}-\mathbf{k}_s|z_f)|V_{Se}\\ &\quad +\frac{V_{SP}}{Z_P}|\Phi_{K_{iz}}^{+}(V_{SP0})\phi_{k_z}^{+}\rangle\\ &= \int \frac{du}{(2\pi)^{1/2}}\tilde{D}_{\rm SVPS}(u)\ \tilde{F}_f^{*}(\mathbf{v}_{fs}-\mathbf{k}_s|W_{fz}+u)\\ &\quad \times \tilde{I}_{k_z}(W_{iz}-u).\end{aligned} \tag{4.24}$$

Note that for $Z_P = 1$, $D_{SP}^{-}(V'_{SP0})$ is unity and the plane wave is recovered. The full expression for $\tilde{D}_{\rm SVPS}$ is

$$\begin{aligned}\tilde{D}_{\rm SVPS}(u) &= \frac{1}{(2\pi)^{1/2}}\int_0^{\infty} dZ \exp(-iuZ)\\ &\quad \times D_{SP}^{-*}(V'_{SP0}, K_{fz};\ Z) D_{SP}^{+}(V_{SP0}, K_{iz};\ Z)\\ &\quad \times\left[1-\frac{2}{(W_{iz}-u)^2-2\epsilon_{iz}}\ \frac{V_{SP}(Z)}{Z_P}\right].\end{aligned} \tag{4.25}$$

An approximation for $\tilde{D}_{\rm SVPS}$ is presented in Appendix D.

V. RESULTS AND DISCUSSIONS

All of the τ-matrix elements developed in the preceding section have the following form:

$$\tau = \int \frac{du}{(2\pi)^{1/2}}\tilde{D}(u)\ \tilde{F}_f^{*}(\mathbf{v}_{fs}-\mathbf{k}_s|W_{fz}+u)\ \tilde{I}_{k_z}(W_{iz}-u), \tag{5.1}$$

or $\tilde{\phi}_f^{*}$ instead of $\tilde{F}_f^{*}$ if first-order theories are considered instead. In practical terms, we use $\tilde{D}_Y^X$ (see Appendixes C and D) and $\tilde{I}_{k_z}^X$ (see Appendix B). Here the superscript X denotes the model; $X = J, M, L$ correspond to the jellium, Molière, and Lindhard models, respectively. The subscript Y represents the approximation Y=B1, SB1, SI, and SVPS, corresponding to the first-order Born, the surface first-order, the surface impulse, and the SVPS approximations, respectively. Although we have made rigorous numerical calculations, we found that there is no appreciable difference if we factor out the integral $\tilde{D}(u)$ evaluated at $u = -W_{fz}$, which is evaluated where $\tilde{F}_f^{*}$ peaks.

Integrating the δ functions contained in $\tilde{I}_{k_z}^X$ (see Appendix B), we obtain

$$\begin{aligned}\tau_Y^X &= -\frac{1}{(2\pi)^{1/2}}\sum_n T_n^X\left[\mathcal{U}H_1(k_z)+\mathcal{R}H_1(-k_z)\right]\\ &\quad +\int \frac{du}{(2\pi)^{1/2}}\tilde{D}_Y^X(u)\ \tilde{F}_f^{*}(\mathbf{v}_{fs}-\mathbf{k}_s|W_{fz}+u)\\ &\quad \times\tilde{\mathcal{I}}_{k_z}^X(W_{iz}-u)\end{aligned} \tag{5.2}$$

$$H_1(k) = \tilde{D}_\gamma^X(W_{iz} - k - 2n\pi/d)$$

$$\times \tilde{F}_f^*(\mathbf{v}_{fs} - \mathbf{k}_s | v_{fz} - k - 2n\pi/d). \quad (5.3)$$

Here we summarize the sources of the quantities used: $\mathcal{U}$, $\mathcal{R}$, and $\mathcal{T}$ are defined in Appendix B [Eq. (B3)] and represent the normalization, the reflection, and the transmission coefficients, respectively; $\tilde{F}_f^*$ has closed form for any final state being given for the ground state by Eq. (4.20); $\tilde{D}^X_{\mathrm{SB1}}$ was derived in the eikonal approximation [Ref. [19], Chap. 9], namely, Eqs. (C4) (with $Z_0 = 0$), (C8), and (C11) for the jellium ($X = J$), Molière ($X = M$), and Lindhard ($X = L$) models, respectively; $\tilde{D}^X_{\mathrm{SVPS}}$ was derived also in the eikonal approximation, namely Eqs. (D1) and (D2) for the Molière ($X = M$) and Lindhard ($X = L$) models, respectively; $\tilde{\mathcal{I}}_{k_z}$ was derived in first perturbative order, namely, Eqs. (B6), (B15), and (B18) for the jellium, Molière, ($X = M$) and Lindhard ($X = L$) models, respectively; and T_n^X are given in Eqs. (B7), (B16), and (B19) for the jellium ($X = J$), Molière ($X = M$), and Lindhard ($X = L$) models, respectively.

The eikonal approximation consists simply of modifying the phase of the undistorted plane wave (see [19], Chap. 9, for details). The numerical calculation involves a single integral on u (which is very cumbersome due to the oscillations introduced by the principal parts; see Appendix B) following a three-dimensional integral over $\mathbf{k}$ space [Eq. (2.19)]. A total probability takes about 1 h in a 10 Mflop computer, the greatest part of the time being spent in the evaluation of the incomplete γ functions.

At this stage, we should we mention *a priori* the com-

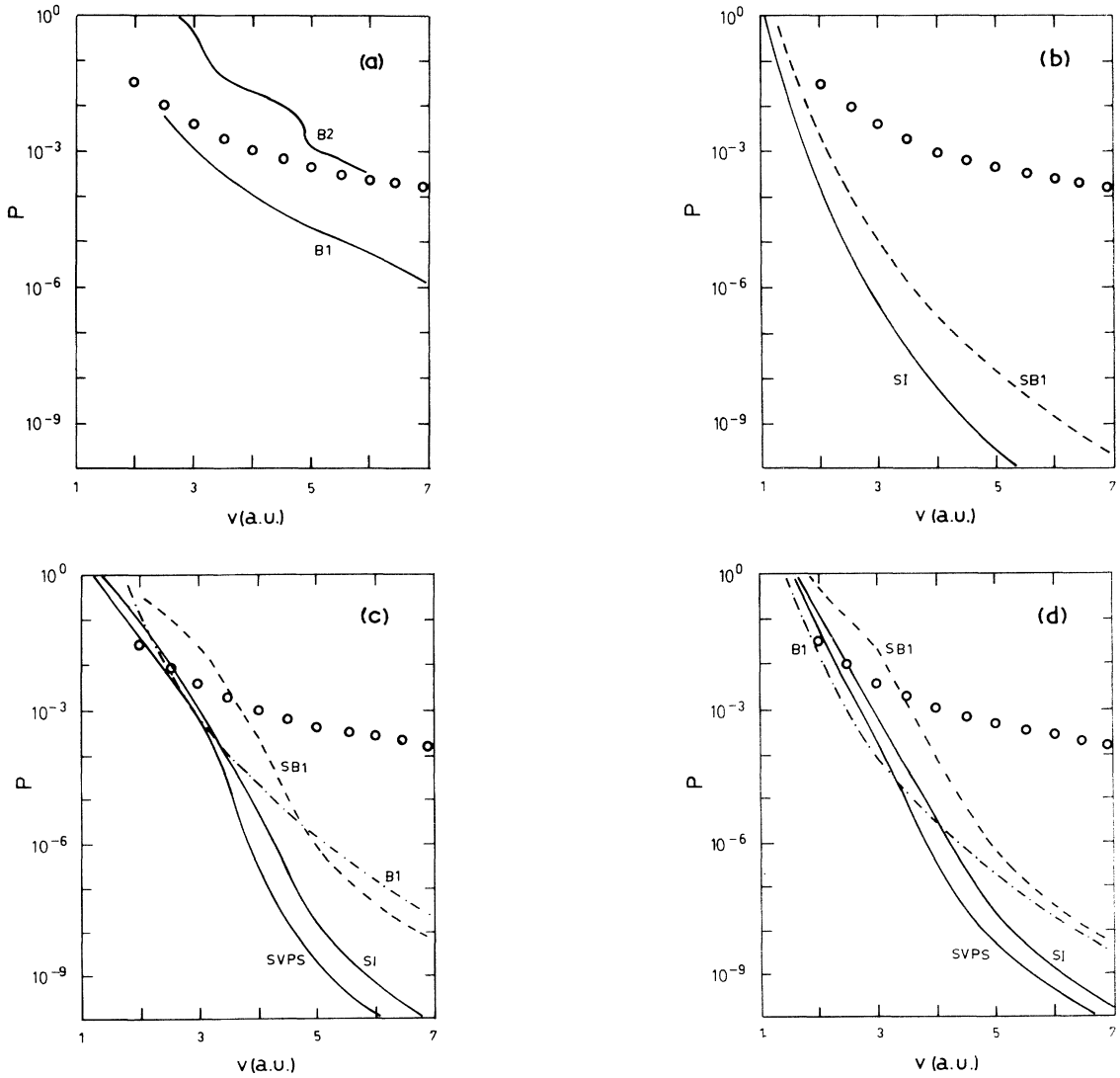

FIG. 6. Total probability for capture by protons from an Al crystal as a function of the incident velocity in a.u. The grazing angle is 3 mrad. The curves are labeled by the corresponding theory and the experiments (open circles) from Winter *et al.* [6] are displayed in all figures. (a) Results of the first- and second-order Born approximations of Thumm and Briggs [2]. (b) Our results for the SB1 and SI, for the jellium model. (c) Our results for B1, SB1, SI, and SVPS for the Molière model. (d) Similar to (c) for the Lindhard model.

parative qualities of the approximations and interactions. In our opinion, the hierarchical order is SVPS > SI > SB1 > B1 for the approximations and M > L > J for the interactions (with the symbol > we mean "better than"). Therefore, the SVPS approximation with the Molière interaction should be the best approximation in the present work.

In Fig. 6(a), we plot the results of TB [2] along with the experiments [6]. In Figs. 6(b), 6(c), and 6(d), we report our results for the jellium, Molière, and Lindhard models, respectively, again including the experiments. As a first observation, we can definitively affirm that there is no agreement at all with the experiments [6], except in the velocity region 2–3 a.u. where the theory crosses the data. In the next subsection, we find some theoretical guidance to discuss in more detail our numerical results.

A. Theoretical tendencies

In this section, we obtain a simple closed form for the probability of electron capture by making *very rough* approximations, from which we will be able to get useful information about the dependence on the main parameters. Let us start with the first order in the B1 approximation as given by Eq. (4.11). We use here the most elemental jellium model to describe the initial electronic wave function, i.e., $\tilde{I}^{J}_{k_z}$ as given by Eq. (B4), a Molière II potential to model the *S-P* interaction, i.e., D^{M}_{B1}, given by Eq. (C3), and final $1s$ state Fourier transform, which is known to be $\varphi_f(K|k) = (8Z_P^5/\pi^2)^{1/2}/(Z_P^2 + K^2 + k^2)$. The resulting integral can be calculated with the Cauchy technique by contouring the complex u plane to give, after some algebra, the following expression:

$$\tau_{\mathrm{B1}} = -2\pi i V_{Ce} V_{SP0} (Z_P/\pi)^{5/2} [\mathcal{U} H_2(k_z) + \mathcal{R} H_2(-k_z)], \tag{5.4}$$

$$\begin{aligned} H_2(k) = {} & \frac{1}{2v_P^2} \frac{1}{(v_{fz} + iv_P)^2 + \gamma_0^2} \frac{1}{v_{fz} - k + iv_P} \frac{1}{W_{fz} + i\kappa_M + iv_P} \\ & \times \left(\frac{1}{iv_P} + \frac{2(v_{fz} + iv_P)}{(v_{fz} + iv_P)^2 + \gamma_0^2} + \frac{1}{v_{fz} + iv_P - k} + \frac{1}{W_{fz} + i\kappa_M + iv_P} \right) \\ & + \frac{1}{[(v_{fz} - i\gamma_0)^2 + v_P^2]^2} \frac{1}{i\gamma_0} \frac{1}{k - i\gamma_0} \frac{1}{v_{fz} - i\gamma_0 - W_{fz} - i\kappa_M}, \end{aligned} \tag{5.5}$$

where $v_P = \left[Z_P^2 + (\mathbf{v}_{fs} - \mathbf{k}_s)^2\right]^{1/2}$ and $\mathcal{U}$, $\mathcal{R}$, and γ_0 are defined in Appendix B.

To obtain a manageable expression in the high velocity limit we proceed to make the following approximations: $M_P \gg 1$, $v_P \approx v_{is} \gg 1$, $|W_{fz}| \gg |v_{iz}|$, to obtain

$$\tau_{\mathrm{B1}} \approx \frac{2iV_{SP0} Z_P^{5/2}}{\pi^{3/2}\, v_{is}^4\, W_{fz}} \mathcal{T}, \tag{5.6}$$

where $\mathcal{T} = \mathcal{R} + \mathcal{U}$ is the transmission factor. This latter parameter takes into account the tunneling mechanism. Integrating $|\mathcal{T}|^2$ over k space as in Eq. (2.19), one obtains

$$\int d\mathbf{k}\, |\mathcal{T}|^2 = \frac{1}{V_{Ce}} \int_{-k_F}^{k_F} dk_z\, k_z^2 (k_F^2 - k_z^2) = \frac{4}{15 V_{Ce}} k_F^5. \tag{5.7}$$

The total probability then behaves as

$$P_{\mathrm{B1}} \approx \frac{2^7 V_{SP0}^2 Z_P^5\, k_F^5}{15\pi S V_{Ce} M_P^2\, v_{is}^8\, v_{iz}^4}, \tag{5.8}$$

where we have introduced the factor

$$S = \frac{v_{fz}}{|v_{iz}|} \left[1 + \frac{v_{fz}}{|v_{iz}|} \right]^2_{k_z \approx 0}. \tag{5.9}$$

The factor S depends on the projectile mass and incident angle evaluated at around $k_z = 0$. Note that the total probability involves a ratio of energies and velocities giving a dimensionless magnitude.

B. Discussion

With the help of the preceding closed-form probability Eq. (5.8), we are able to study the dependence of our numerical results on the collision parameters. We summarize the main features.

(i) For $1s$-$1s$ electron capture in ion-atom collision, the first-order BK approximation behaves in the high-energy limit as $Z_P^5 Z_T^5$, where Z_T is the target charge [8]. Our model predicts the same dependence on k_F instead of Z_T.

(ii) At the level of the differential probability dP/dk_z, we have found that our numerical calculations (not shown here) follow indeed a shape similar to $k_z^2(k_z - k_F)^2$, as predicted by Eq. (5.7).

(iii) If we consider, as in the experiment of Winter *et al.* [6], that the transverse velocity satisfies $v_{iz} \propto v_i$, we discover that the probability varies as $v_{iz}^{-4} v_{is}^{-8} \propto v_i^{-4} v_i^{-8} = v_i^{-12}$ in a similar fashion to the Brinkman-Kramers counterpart in ion-atom collisions. The first-order SB1 curves as plotted in Fig. 6 vary as $v_i^{-12.5}$, $v_i^{-13.8}$, and $v_i^{-13.6}$, for the jellium, Molière, and Lindhard potentials, respectively, in the range $v_i = 6 - 7$ a.u. So the dependence v_i^{-12} seems to be quite near the numerical one.

(iv) Furthermore, the probability falls off as v_{iz}^{-4} in agreement with the prediction of Dettmann and Leibfreid for backward capture in their one-dimensional model [Eq.

(22) of Ref. [20]].

(v) From Fig. 6, it can be observed that the distorted wave methods SI and SVPS fall off faster than the first-order B1 and SB1 approximations. The explanation is simple. The only difference with the first order approximation is the presence of the modulating factor $M(u)$ [see Eq. (4.20)]. It is composed of three terms: the Coulomb factor $[\exp(\pi a_P/2)\,\Gamma(1-ia_P)]$ and the term $A_P^{-ia_P}$, both of which tend to unity as $v_{is}\to\infty$, and the third factor within squared brackets, which contains a key variable A_P. This can be approximated by

$$A_P \approx \frac{(k_z - W_{iz} + u)^2 - (v_r + iZ_P)^2}{v_r^2 + Z_P^2 + (W_{fz} + u)^2}, \tag{5.10}$$

where we have considered, when convenient, $v_{is}\approx v_{fs}\approx v_r \gg k_s$ and $M_P \gg 1$. The main contribution to the u integral Eq. (4.18) comes from the region $u\approx W_{fz}$, so A_P takes the value

$$A_P(u\approx W_{fz}) \approx \frac{1+ia_P}{1-ia_P} - \frac{(k_z - v_{iz})^2}{v_r^2} \tag{5.11}$$

and we find

$$M(u\approx W_{fz}) \propto \frac{1}{v_r^2} = O(v_{is}^{-2}). \tag{5.12}$$

We conclude that the T matrix may fall off faster than the first order approximation (either B1 or SB1) because of a factor $O(v_{is}^{-2})$. Investigating our numerical results in the range $v_i = 6-7$ a.u. we fit the SI values with $v_i^{-13.9}$, $v_i^{-15.2}$, and $v_i^{-14.4}$, for the jellium, Molière, and Lindhard potentials, respectively. So at the level of total probability, our distorted wave results fall off faster than the first order approximation, in total contrast to the finding of TB [2].

Of course, the SI and SVPS also include two-step processes due to the Thomas mechanism (occurring when $\mathrm{Re}A_P = 0$), but it does not give rise to steplike structures at the level of total probability as found by TB [2] [see curve B2 in Fig. 6(a)].

VI. CONCLUSIONS

In this article, we have developed a quantum formalism to treat electron capture from crystal surfaces by heavy projectiles at grazing incidence. After modeling the interactions involving the surface, we have adapted some theoretical methods commonly used in three-particle atomic collision theory, namely, two first-order approximations (B1 and SB1) and two distorted-wave methods (SI and SVPS), taking into account part of the second-order Born approximation, which is known to be dominant in rearrangement collisions. In synthesis, our work adapts the outstanding distorted-wave methods developed in atomic collision theory during the past sixty years.

Approximations were used to evaluate the quantities $\tilde{D}$ (see Appendixes C and D) and $\tilde{I}_k$ (see Appendix B), and these are uncertain points. Much should be done to better calculate $\tilde{D}$, which, we suspect, is the weakest aspect of the evaluation.

As far as capture by protons from the electron gas of the Al crystal is concerned, we summarize the main points of this article.

(i) The outgoing transverse velocity v_{fz} is found to be larger than the incoming one $|v_{iz}|$, in contrast to the specular trajectory approximation. This point would be interesting to study if the final angular distribution were measured.

(ii) First-order approximations such as B1 and SB1 fall off approximately as $\sim v^{-12}$.

(iii) Higher-order approximations such as SI and SVPS fall off faster and always run below the first orders.

(iv) There is no substantial difference whether we use the Lindhard or Molière potential.

(v) Huge differences are observed when compared with the experiments of Winter *et al.* [6] and the theories developed by TB [2] in the high-energy tail. Furthermore, steplike structures as in the theoretical work of TB [2] are not observed.

(vi) The only theory that overlaps the experiments of Winter *et al.* [6] is the SVPS approximation using the Molière model and even then only in the region $v_i = 2-3$ a.u. It is significant that this involves the most elaborate theoretical method and the trustiest potential. At higher velocities $v_i > 3$ a.u., the theory presents no impediments to be used; furthermore, the larger the impact velocity, the more reliable the theory should be. At lower velocities $v_i < 2$ a.u., all the theories developed here are out of the range of validity, and a proof of that is that the probability is larger than unity.

In summary, we show that theoretical estimates for capture from the free-electron gas at high energies largely underestimate the experiments Winter *et al.* [6]. Other mechanisms should be studied to explain these experiments. In the following article [17] we study the capture from bound states of atoms which form the surface.

ACKNOWLEDGMENTS

I would like to thank M.S. Gravielle for useful comments.

APPENDIX A: EVALUATION OF THE SURFACE POTENTIAL

The S-e interaction can be approximated by

$$V_{Se}(z) = \delta_s \int d\rho\; V\left[r = (z^2+\rho^2)^{1/2}\right], \tag{A1}$$

where $V(r)$ is the potential between one atom of the surface and the electron, $\delta_s = \delta_V\, d$ is the density of atoms in the surface, δ_V is the density of atoms per unit volume, and d is the separation of the crystal planes. Two analytical approximations to the Thomas-Fermi atomic potential will be considered thorough this work: the Molière and Lindhard [9] simple forms given by

$$V(r) = \begin{cases} -\frac{Z_T}{r}\sum_j a_j \exp(-b_j\, r/a_e), & \text{Molière} \\ -\frac{Z_T}{r}\left[1 - \frac{1}{(1+(c\,a_e/r)^2)^{1/2}}\right], & \text{Lindhard}, \end{cases} \tag{A2}$$

where $a_e = 0.8853/(Z_T^{2/3}+1)^{1/2}$ and $c^2 \approx 3$. The Molière parameters are $a_1 = 0.35$, $a_2 = 0.55$, $a_3 = 0.10$, $b_1 = 0.30a_e$, $b_2 = 1.2a_e$, and $b_3 = 6.0a_e$. The Molière form has been one of the most popular potential used in the past and it is known to fail at large separations. On the other hand, the Lindhard expression gives a good account of the potential at intermediate and large distances and it has been largely used in string and planar channeling [23]. It fails at very large separation because it falls off as $1/r^3$ while the exact Thomas-Fermi falls off as $1/r^4$. This failure has serious implications here because, as we shall see, the corresponding planar potential falls off as $1/z$, giving rise to a conflicting Coulomb potential [see Eq. (A4)].

After doing the surface integral (A1), the S-e interactions then read

$$V_{Se}(z) = \begin{cases} -V_{Se0}/c \sum_j \dfrac{a_j}{b_j} \exp(-b_j\, z/a_e), & \text{Molière I} \\ -V_{Se0} \left[\left[1 + \left(\dfrac{z}{ca_e} \right)^2 \right]^{1/2} - \dfrac{z}{ca_e} \right], & \end{cases}$$

Lindhard I, (A3)

where $V_{Se0} = 2\pi Z_T \delta_s a_e c$. Results for electrons in aluminum crystal are shown in Fig. 3; the parameters are $Z_T = 13$, $\delta_s = 0.0337$, and $a_e = 0.3464$, and so $V_{Se0} = 1.66$. None of those potentials have known quantum-mechanical solutions. Some approximations are performed next.

In the Molière case, we approximate $\sum_j a_j/b_j \exp(-zb_j/a_e) = c \exp(-\kappa_m z)$, where $c = \sum_j a_j/b_j$. In the Thomas-Fermi potential $\kappa_m \propto 1/a_e$. The use of a single exponential is equivalent to the Bohr potential [9]. This potential decays very rapidly with increasing r, becoming invalid at separations greater than few atomic units (Ref. [9], p. 58). In the Lindhard case, we replace the expression within squared brackets by a Coulomb-type expression.

In this way, we will work with two approximate potentials (labeled with II to differentiate them from the authentic ones, labeled with I) given by

$$V_{Se}(z) = \begin{cases} -V_{Se0} \exp[-\kappa_m z], & \text{Molière II} \\ -V_{Se0} \left[1 + \kappa_l z \right]^{-1}, & \text{Lindhard II.} \end{cases} \quad \text{(A4)}$$

As we shall see in Appendix C, the continuum wave functions corresponding to the Molière II and Lindhard II potentials can be related to the hypergeometric functions ${}_0F_1$ and ${}_1F_1$, respectively

Now we proceed to determine $\kappa_{l,m}$ to satisfy the experimental confinement potential $V_{Ce} = E_F + E_W$, where E_F and E_W are the Fermi energy and the work function. According to the model used (see Sec. III and Fig. 4), we impose $V_{Se}(d/2) = V_{Ce}$ and then

$$\kappa_m \approx \frac{2}{d} \ln \frac{2V_{Se0}}{V_{Ce}}, \qquad \kappa_l = \frac{2}{dV_{Ce}} (2V_{Se0} - V_{Ce}). \quad \text{(A5)}$$

For an aluminum crystal, $V_{Ce} = 0.59$, and $d = 3.8$ a.u., and so $\kappa_m = 0.92$ and $\kappa_l = 2.47$. In Fig. 3, we show the S-e Molière II and Lindhard II potentials using these parameters, which agree quite well with the original Molière I and Lindhard I potentials, respectively.

We have also explored the Hartree-Fock approximation producing the following the static potential:

$$V(r) = -\frac{Z_T}{r} + \sum_{n,l,m} \int d\mathbf{x} \frac{|\phi_{nlm}(\mathbf{x})|^2}{|\mathbf{x} - \mathbf{r}|}. \quad \text{(A6)}$$

By using the single z function [11] to represent the bound states ϕ_{nlm} and performing the integral (A1) we obtain the surface potential labeled with HI in Fig. 3. The curve can be fairly fitted with the simple expression $1.4 \exp(-1.3\ z)$ as shown in Fig. 3 with a dashed line denoted with HII. For $z < 2$ all the curves run near each other, but for $z \geq 2$ huge differences are observed.

APPENDIX B: EVALUATION OF $\tilde{I}_K$ IN FIRST PERTURBATIVE ORDER

We have to solve the Schrödinger equation of the electron interacting with a one-dimensional crystal through a semiperiodic potential $V_{Se}(z)$ as described in Sec. III. When obtained the solution $\phi_k^+(z)$, the magnitude of interest here is

$$\begin{aligned} \tilde{I}_k(W) &= \int_{-\infty}^{+\infty} \frac{dz}{(2\pi)^{1/2}} \exp(-iWz)\ \phi_k^+(z)\ V_{Se}(z) \\ &= \left[\epsilon_{iz} - W^2/2 \right] \tilde{\phi}_k^+(W). \end{aligned} \quad \text{(B1)}$$

1. Jellium model

We start calculating $\tilde{I}_k$ in the jellium model, where the wave function is simply [2]

$$\phi_k^{+(J)}(z) = \begin{cases} \mathcal{U} \exp(ikz) + \mathcal{R} \exp(-ikz), & z < 0 \\ \mathcal{T} \exp(-\gamma_0 z), & z > 0, \end{cases} \quad \text{(B2)}$$

where

$$\mathcal{U} = \frac{1}{(2\pi)^{1/2}}, \qquad \mathcal{R} = \mathcal{U} \frac{k - i\gamma_0}{k + i\gamma_0}, \quad \mathcal{T} = \mathcal{U} \frac{2k}{k + i\gamma_0},$$

$$\gamma_0 = (2V_{Ce} - k^2)^{1/2}, \quad \text{(B3)}$$

and $\mathcal{U}$, $\mathcal{T}$, and $\mathcal{R}$ denote the normalization, transmission, and refraction coefficients, respectively. After simple algebra, we find

$$\tilde{I}_k^J(W) = -\frac{iV_{Ce}}{(2\pi)^{1/2}} \left[\frac{\mathcal{U}}{W - k + i\eta} + \frac{\mathcal{R}}{W + k + i\eta} \right]. \quad \text{(B4)}$$

Since $\tilde{I}_k$ is within an integral operation, it is convenient to extract the δ functions to give

$$\tilde{I}_k^J(W) = -T_0^J\,[\mathcal{U}\delta(W-k) + \mathcal{R}\delta(W+k)] + \tilde{\mathcal{I}}_k^J(W), \tag{B5}$$

$$\tilde{\mathcal{I}}_k^J(W) = -\frac{iV_{Ce}}{(2\pi)^{1/2}}\left[\mathcal{U}\,\mathcal{P}_1^{(-)}(W) + \mathcal{R}\,\mathcal{P}_1^{(+)}(W)\right], \tag{B6}$$

$$T_0^J = V_{Ce}(\pi/2)^{1/2}, \tag{B7}$$

$$\mathcal{P}_1^{(\pm)}(W) = \mathrm{P}\left[\frac{1}{W\pm k}\right] = \frac{W\pm k}{(W\pm k)^2+\eta^2}, \tag{B8}$$

where P denotes the principal part.

For any other potential V_{Se}^X, we can iterate the Schrödinger equation starting from the jellium potential V_{Se}^J as developed by Bethe and Salpeter [28]. In general, we can write

$$\tilde{I}_{\mathbf{k}}^X(W) = \tilde{I}_{\mathbf{k}}^J(W) + \int_{-\infty}^{+\infty}\frac{dz}{(2\pi)^{1/2}}\exp(-iWz)\,\phi_k^{+(J)}(z) \times[V_{Se}^X(z) - V_{Se}^J(z)]\,, \tag{B9}$$

where $X = J$, M, and L denote the potential, namely, the jellium [Eq. (3.1)], Molière [Eq. (3.2)], and Lindhard [Eq. (3.3)] models, respectively. In this way, we obtain $\tilde{I}_{\mathbf{k}}^X$ in first perturbative order in the potential $V_{Se}^X(z) - V_{Se}^J(z)$.

2. Molière model

In this case, the integral (B9) can be easily performed and we find, after some algebra,

$$I_k^M(W) = \frac{iV_{Se0}}{(2\pi)^{1/2}}\Big[\frac{\mathcal{T}}{W-i(\kappa_m+\gamma_0)} - \frac{\mathcal{U}}{(W-k)-i\kappa_m} - \frac{\mathcal{R}}{(W+k)-i\kappa_m}\Big] - \frac{2V_{Se0}\kappa_m}{(2\pi)^{1/2}}\Big[\frac{\mathcal{U}C^{(-)}(W)}{(W-k)^2+\kappa_m^2} + \frac{\mathcal{R}C^{(+)}(W)}{(W+k)^2+\kappa_m^2}\Big], \tag{B10}$$

where $C^{(\pm)}(W)$ are the one-dimensional crystal factors

$$C^{(\pm)}(W) = \sum_{j=0}^{\infty}\exp\{-[\epsilon_c - i(W\pm k)]jd\} \tag{B11}$$

and we have introduced $\epsilon_c \to 0^+$ to make the series convergent. The sum on j can be then solved in closed form to give

$$C^{(\pm)}(W) = \{1-\exp[-\epsilon_c d + i(W\pm k)d]\}^{-1} = i\mathcal{P}_2^{(\pm)}(W) + \frac{\pi}{d}\sum_N \delta(\pm k - 2N\pi/d), \tag{B12}$$

$$\mathcal{P}_2^{(\pm)}(W) = \mathrm{P}\left[\frac{1}{i - i\exp[i(W\pm k)]d]}\right], \tag{B13}$$

with $\epsilon_c d \to 0$. Factoring out the δ functions, we obtain, in similar fashion to Eq. (B5),

$$I_k^M(W) = -\sum_{n=0}^{\infty} T_n^M\,[\mathcal{U}\delta(W-k-2n\pi/d) + \mathcal{R}\delta(W+k-2n\pi/d)] + \tilde{\mathcal{I}}_k^M(W), \tag{B14}$$

with

$$\tilde{\mathcal{I}}_k^M(W) = \frac{i\mathcal{T}V_{Se0}}{(2\pi)^{1/2}[W-i(\kappa_m+\gamma_0)]} - \frac{iV_{Se0}}{(2\pi)^{1/2}} \times\Big[\mathcal{U}\frac{1}{W-k-i\kappa_m} + 2\kappa_m\mathcal{U}\mathcal{P}_2^{(-)}(W)M^{(-)}(W) + \mathcal{R}\frac{1}{W+k-i\kappa_m} + 2\kappa_m\mathcal{R}\mathcal{P}_2^{(+)}(W)M^{(+)}(W)\Big], \tag{B15}$$

$$T_n^M = \frac{V_{Se0}(2\pi)^{1/2}}{\kappa_m d}\left[\frac{\kappa_m^2 d^2}{4n^2\pi^2+\kappa_m^2 d^2}\right], \tag{B16}$$

and $M^{(\pm)}(W) = [(W\pm k)^2+\kappa_m^2]^{-1}$.

3. Lindhard model

Following the same pattern as before, we obtain, after tedious algebra,

$$I_k^L(W) = -\sum_{n=0}^{\infty} T_n^L\Big[\mathcal{U}\delta(W-k-2n\pi/d) + \mathcal{R}\delta(W+k-2n\pi/d)\Big] + \tilde{\mathcal{I}}_k^L(W), \tag{B17}$$

where

$$\tilde{\mathcal{I}}_k^L(W) = -\frac{V_{Se0}}{(2\pi)^{1/2}\kappa_l}[\mathcal{T}E_0 - \mathcal{U}E(x^{(-)}) - \mathcal{R}E(x^{(+)}) + 2i\mathcal{U}\mathcal{P}_2^{(-)}(W)\mathrm{Re}E(x^{(-)}) + 2i\mathcal{R}\mathcal{P}_2^{(+)}(W)\mathrm{Re}E(x^{(+)})], \tag{B18}$$

$$T_n^L = \frac{V_{Se0}(2\pi)^{1/2}}{\kappa_l d}\mathrm{Re}E(x^{(n)}), \tag{B19}$$

$x_0 = (\gamma_0 + iW)/\kappa_l$, $x^{(n)} = [\eta d + i2n\pi]/(\kappa_l d)$, $x^{(\pm)} = [\eta + i(W\pm k)]/\kappa_l$,

$$E_0 = \exp(x_0)\,E_1(x_0), \qquad E(x) = \exp(x)[E_1(x) - E_1(x + xd\kappa_l)], \tag{B20}$$

E_1 is the exponential integral and Re denotes the real part.

APPENDIX C: EVALUATION OF $\tilde{D}_{SB1}$ IN THE EIKONAL APPROXIMATION

To obtain this magnitude, we first solve the one-dimensional Schrödinger equation

$$\left(-\frac{1}{2M_P}\frac{d^2}{dZ^2}+V_{SP}(Z)-\frac{K^2}{2M}\right)\Phi_K^{\pm}(V_{SP0};Z)=0. \tag{C1}$$

If we then write

$$\Phi_K^{\pm}(V_{SP0};Z)=\exp(iKZ)D_{SP}^{\pm}(V_{SP0},K;Z)/(2\pi)^{1/2},$$

the function $D_{SB1}(Z)$ is defined as $D_{SB1}(Z) = D_{SP}^{+}(V_{SP0},K_{iz};Z)D_{SP}^{-*}(V_{SP0},K_{fz};Z)$. $D_{SP}^{\pm}(Z)$ is generally a difficult expression to handle. For $Z>0$, $D_{SP}^{\pm}(Z)$ is composed of four terms: two of them contain very oscillating functions, such as $\exp(2iK_{iz}Z)$ and $\exp(2iK_{fz}Z)$, and so they can be dropped, as far as heavy projectiles are concerned. The third term takes into account interferences between the incoming and outgoing projectile waves giving rise to an exponential of the type $\exp[2i(K_{iz}-K_{fz})Z]$, and it will also be neglected. The remaining term is the product of the incoming distortion for negative times and the outgoing distortion for positive times; throughout this work, we have evaluated only this term. For grazing collisions, the most relevant contribution comes from the interaction of the projectile with outermost surface of the crystal and so we define

$$\tilde{D}_{SB1}(u)=\int_0^{\infty}\frac{dZ}{(2\pi)^{1/2}}\exp(-iuZ)\,D_{SB1}(Z), \tag{C2}$$

where $D_{SB1}(Z)$ is the solution for $Z>0$. We integrate from $Z=0$ simply because the transmission is small and therefore the probability of penetration is negligible. Mathematically, this can be seen by inspecting the eikonal approximations [see Eqs. (C6) and (C10)]; the strong oscillatory behavior cancels most of the information for Z less than the turning point.

Accordingly, we define the corresponding Fourier transform, of the potential also in the outside region ($Z>0$) to obtain

$$\tilde{V}_{B1}^{M}(u)=\frac{V_{SP0}}{(2\pi)^{1/2}(\kappa_M+iu)},$$
$$\tilde{V}_{B1}^{L}(u)=\frac{V_{SP0}\exp(iu/\kappa_L)}{(2\pi)^{1/2}\kappa_L}\,E_1(iu/\kappa_L) \tag{C3}$$

for the Molière and Lindhard cases, respectively, and E_1 is the exponential integral. In mathematical terms, this is equivalent to considering $V_{SP}(Z)$ for $Z>0$ and zero otherwise (see Fig. 4). Note that both $\tilde{V}_{B1}^{M}$ and $\tilde{V}_{B1}^{L}$ tend to $V_{SP0}/[(2\pi)^{1/2}iu]$ as $u\to\infty$. Therefore, for large momentum transfers, i.e., $u\sim -W_{fz}\gg 1$, both models should coincide.

1. Unpenetrable wall model

First, we consider the S-P interaction described by an unpenetrable wall at Z_0 used by TB [2]. In this case, one simply finds

$$\tilde{D}_{SB1}^{J}(u)=\frac{1}{(2\pi)^{1/2}}\frac{\exp[-(\eta+iu)Z_0]}{\eta+iu}. \tag{C4}$$

We are going to use this model to describe the S-P interaction with the jellium model describing the S-e interaction, which is why we use the superscript J. For simplicity, we consider $Z_0=0$, that is, the projectile reflects in the outermost surface coinciding with the contention barrier of the electrons in the jellium model.

2. Molière model

For this case, $D_{SP}^{\pm}(V_{SP0},K;Z)$ has closed form in terms of the hypergeometric function ${}_0F_1$. For $|Z|>0$, and neglecting the interferences with the reflected waves as mentioned before, we obtain

$$D_{SB1}^{M}(Z)={}_0F_1\left[1+i\alpha_f,\beta^2\exp(-Z\kappa_M)\right]\times{}_0F_1\left[1+i\alpha_i,\beta^2\exp(-Z\kappa_M)\right], \tag{C5}$$

with $\alpha_{i,f}=+2|K_{iz,fz}|/\kappa_M$, $\beta^2=2M_PV_{SP0}/\kappa_M^2$, and the superscript M denotes the Molière model used.

The partial Fourier transform of Eq. (C5) can be expressed in terms of the generalized hypergeometric function ${}_3F_4$ [26], but its manipulation is very cumbersome to deal with. It can be shown that the eikonal approximation produces (see Ref. [19], Chap. 9)

$$D_{SB1}^{M}(Z)=\exp\left[-\Lambda_M\exp(-\kappa_MZ)\right] \tag{C6}$$

with

$$\Lambda_M=-i\frac{\beta^2\kappa_M}{2}\left(\frac{1}{|K_{iz}|}+\frac{1}{K_{fz}}\right) \tag{C7}$$

and $\lambda_M=(\eta+iu)/\kappa_M$. The Fourier transform reads

$$\tilde{D}_{SB1}^{M}(u)=\frac{1}{\kappa_M(2\pi)^{1/2}}\Lambda_M^{-\lambda_M}\gamma(\lambda_M,\Lambda_M), \tag{C8}$$

where γ is the incomplete gamma function [Eq. (6.5.12) of Ref. [27]]. This is an expression relatively simple to manipulate within an integral operation.

3. Lindhard model

$D_{SB1}^{L}(Z)$ can be calculated in closed form and it is expressed in terms of the hypergeometric functions ${}_1F_1$

$$\begin{aligned}D_{SB1}^{L}=&-\exp\left[-(N_f+N_i)\pi/2\right]\,\Gamma(1+iN_f)\Gamma(1+iN_i)\\&\times i2K_{fz}(Z+1/\kappa_L){}_1F_1\left[1-iN_f,\,2,2iK_{fz}(Z+1/\kappa_L)\right]\\&\times i2K_{iz}(Z+1/\kappa_L){}_1F_1\left[1-iN_i,\,2,-2iK_{iz}(Z+1/\kappa_L)\right],\end{aligned} \tag{C9}$$

with $N_{i,f} = MV_{SP0}/(|K_{iz,fz}|\kappa_L)$ and $Z > 0$. This expression is again difficult to handle. The eikonal form produces a simpler one given by (except a factor phase)

$$D^L_{\rm SB1} = [1 + \kappa_L Z]^{i(N_i+N_f)}, \tag{C10}$$

and so

$$\tilde{D}^L_{\rm SB1}(u) = \frac{1}{\kappa_L(2\pi)^{1/2}} \lambda_L^{-\Lambda_L} \exp(\lambda_L)\Gamma(\Lambda_L, \lambda_L), \tag{C11}$$

where Γ is the incomplete gamma function [Eq. (6.5.3) of Ref. [27]], $\lambda_L = (\eta + iu)/\kappa_L$, and $\Lambda_L = 1 + i(N_i + N_f)$. Obviously, one can show that the eikonal expression Eq. (C10) is simply the asymptotic limit of Eq. (C9) for large Z.

APPENDIX D: EVALUATION OF $\tilde{D}_{\rm SVPS}$ IN THE EIKONAL APPROXIMATION

If we use the eikonal approximation as developed in Appendix C, closed forms can be obtained as follows.

1. Molière model

$$\tilde{D}^M_{\rm SVPS}(u) = \frac{1}{\kappa_M(2\pi)^{1/2}} \Lambda_M'^{(-\lambda_M)} \gamma(\lambda_M, \Lambda'_M) - \frac{2}{(W_{iz}-u)^2 - 2\epsilon_{iz}} \frac{V_{SP0}}{Z_P \kappa_M (2\pi)^{1/2}} \times \Lambda_M'^{(-\lambda'_M)} \gamma(\lambda'_M, \Lambda'_M), \tag{D1}$$

$$\Lambda'_M = -i\frac{\beta^2 \kappa_M}{2}\left(\frac{1}{|K_{iz}|} + \frac{Z_P - 1}{Z_P K_{fz}}\right), \tag{D2}$$

and $\lambda'_M = (\kappa_M + iu)/\kappa_M$.

2. Lindhard model

$$\tilde{D}^L_{\rm SVPS}(u) = \frac{1}{\kappa_L(2\pi)^{1/2}} \lambda_L^{-\Lambda'_L} \exp(\lambda_L)\Gamma(\Lambda'_L, \lambda_L) - \frac{2}{(W_{iz}-u)^2 - 2\epsilon_{iz}} \frac{V_{SP0}}{Z_P \kappa_L (2\pi)^{1/2}} \times \lambda_L^{-\Lambda''_L} \exp(\lambda_L)\Gamma(\Lambda''_L, \lambda_L), \tag{D3}$$

$$\Lambda'_L = 1 + \Lambda''_L, \qquad \Lambda''_L = i\left(N_i + \frac{Z_P - 1}{Z_P} N_f\right). \tag{D4}$$

[1] J. Burgdörfer, E. Kupfer, and H. Gabriel, Phys. Rev. A **35**, 4963 (1987).
[2] U. Thumm and J. Briggs, Nucl. Instrum. Methods B **43**, 471 (1989).
[3] U. Thumm and J. Briggs, Nucl. Instrum. Methods B **40/41**, 161 (1989).
[4] U. Thumm, J. Phys. B **25**, 421 (1992).
[5] H. J. Andrä, in *Fundamental Processes of Atomic Dynamics*, Vol. 181 of *NATO Advanced Study Institute, Series B: Physics*, edited by J. S. Briggs, H. Kleinpoppen, and H. O. Lutz (Plenum, New York, 1988).
[6] H. Winter, R. Kirsch, J. Poizat, and J. Remillieux, Phys. Rev. A **43**, 1660 (1991).
[7] Dz. Belkic, R. Gayet, and A. Salin, Phys. Rep. **56**, 279 (1979).
[8] K. Dettmann, in *Springer Tracts in Modern Physics*, edited by G. Hohler (Springer, Berlin, 1971), Vol. 58, p. 119.
[9] I. M. Torrens, Interatomic Potentials (Academic, New York, 1972).
[10] In the very particular case that the range of the potential is very short, we could use $V_{Se}(z) = -V_{Ce} - (V_{Se0} - V_{Ce}) \sum_{j=0}^{\infty} \exp[-\kappa_m|z + jd|]$.
[11] C. Clementi and C. Roetti, At. Data Nucl. Data Tables **14**, 445 (1974), Table 43.
[12] H. C. Brinkman and H. K. Kramers, Proc. Acad. Sci. Amsterdam **33**, 973 (1930).
[13] J. D. Jackson and H. Schiff, Phys. Rev. **89**, 359 (1953).
[14] G. F. Chew, Phys. Rev. **80**, 196 (1950).
[15] J. Briggs, J. Phys. B **10**, 3075 (1977).
[16] L. Vainstein, L. Presnyakov, and I. Sobelman, Zh. Eksp. Teor. Fiz. **45**, 2015 (1964) [Sov. Phys. JETP **18**, 1383 (1964)].
[17] M. S. Gravielle and J. E. Miraglia, following paper, Phys. Rev. A **50**, 2425 (1994).
[18] M. L. Golberger and K. Watson, *Collision Theory* (Wiley, New York, 1964).
[19] C. H. Joachain, *Quantum Collision Theory* (North-Holland, Amsterdam, 1979), p. 378.
[20] K. Dettmann and G. Leibfried, Z. Phys. **210**, 43 (1968).
[21] S. Geltman, J. Phys. B **4**, 1288 (1971).
[22] Dz. Belkic and A. Salin, J. Phys. B **9**, L397 (1976).
[23] J. E. Miraglia, R. Gayet, and A. Salin, Europhys. Lett. **6** (5), 397 (1988).
[24] Dz. Belkic, J. Hanssen, R. Gayet, and A. Salin, J. Phys. B **19**, 2945 (1986).
[25] J. P. Dewangan and J. Eichler, J. Phys. B **19**, 2939 (1986).
[26] Y. L. Luke, *The Special Functions and Their Approximations* (Academic, New York, 1969), Vol. I, p. 58.
[27] *Handbook of Mathematical Functions*, edited by M. Abramowitz and I. A. Stegun (Dover, New York, 1972).
[28] H. Bethe and E. E. Salpeter, *Quantum Mechanics of One- and Two-Electron Atoms* (Springer, Berlin, 1957).